IOP Publishing Journal of Physics B: Atomic, Molecular and Optical Physics
J. Phys. B: At. Mol. Opt. Phys. **54** (2021) 185201 (7pp) https://doi.org/10.1088/1361-6455/ac2c8b

Formation of negative-ion resonance and dissociative attachment in collisions of NO_2 with electrons

Hainan Liu[1,2], Xianwu Jiang[1,3], Chi-Hong Yuen[4,5,*], Viatcheslav Kokoouline[4] and Mehdi Ayouz[1,*]

[1] Université Paris-Saclay, CentraleSupélec, Laboratoire LGPM, 91190, Gif-sur-Yvette, France
[2] Department of Basic Courses, Naval University of Engineering, Wuhan, 430033, People's Republic of China
[3] School of Science, Wuhan University of Technology, Wuhan 430070, People's Republic of China
[4] Department of Physics, University of Central Florida, 32816, FL, United States of America
[5] Department of Physics, Kansas State University, Manhattan, KS 66506, United States of America

E-mail: iyuen@phys.ksu.edu and mehdi.ayouz@centralesupelec.fr

Received 13 April 2021, revised 20 September 2021
Accepted for publication 4 October 2021
Published 26 October 2021

Abstract

The process of electron attachment to the NO_2 molecule is investigated theoretically using an approach based on a study by O'Malley (1966 *Phys. Rev.* **150** 14). The approach combines the normal mode approximation for representation of vibrational dynamics of NO_2 and one-dimensional treatment, along each normal mode, of the attachment process as in O'Malley's theory, such that only a modest computational effort is required to compute the attachment cross section. Taking into account the survival probability of the formed resonant state of NO_2^-, the cross section for dissociative electron attachment to NO_2 is also estimated. To compare with available experimental data, the theoretical cross section is convoluted with energy distribution of NO_2–e^- collisions with uncertainties reported in experimental studies. Peak values of the convoluted theoretical cross section are found to be about a factor of 2–10 larger than the experimental results.

Keywords: dissociative attachment, NO_2 molecule, electron attachment, *R*-matrix, normal mode approximation

(Some figures may appear in colour only in the online journal)

1. Introduction

NO_x molecules (NO and NO_2) have detrimental effects on the human respiratory system and the environment. The species are produced and released in large quantities by coal-based power plants and diesel engines. This is the reason why there is a significant interest in technologies able to remove the species from the power plant flue and engine exhaust gases and, often, from the air in ventilation systems. Current technologies frequently used for removal of NO_x are based on creating plasma from major constitutes of the flue gas such as N_2, O_2, and CO_2 to react with NO_x. Electron beam technology for pollution control is gaining research interests in recent years due to its effectiveness [1–3]. However, due to its high cost of operation [1, 4], this technology is still in an early stage for commercialization even though it reduces NO_x with an efficiency of more than 90%. Extensive investigations have been carried out to search for an efficient and cost-effective solution. Recently, a study [5, 6] has demonstrated that it is possible to remove the NO_x molecule with efficiency more than 95%. However, in the mentioned study a pulsed electron beam carrying energy about 500 keV was used. For a comparison, a typical electronic resonance in electron–molecule spectrum

* Authors to whom any correspondence should be addressed.

of dissociative attachment requires only a few eV to be activated. Activating such resonances would lead the molecule, via a resonant state of the negative molecular ion, to dissociation, i.e. to the removal of the molecule from the environment. If one can employ this process of dissociative electron attachment (DEA) to destroy NO_x, then it would be possible to significantly reduce the power cost of pollution reduction using the electron beam technology. In addition, NO_2 gas can be used for decontamination in food processing [7]: it has been shown that NO_2 cold plasma can kill *Escherichia coli* bacterium effectively [8] and the fragments produced by DEA to NO_2 in the plasma may play a critical role. As a result, it is important to understand the mechanism of the DEA process in NO_2.

DEA to NO_2 has been studied experimentally for decades [9–15]. The cross section to the dominant $NO + O^-$ channel, measured in reference [12], shows a peak located at the electron scattering energy of 1.6 eV. The peak was attributed to the $^3B_1$ and $^1B_1$ resonant states of NO_2^-. Rangwala *et al* [13] found peaks of cross sections for formation of the O^- fragment around 1.4 eV, 3.0 eV, and 8.2 eV. In the experiment by Nandi *et al* [14], the resonances at 1.8 and 3.5 eV in the O^- channel for the e^-–NO_2 system appear to have same dissociation channel of $NO + O^-$. Therefore, there is a consensus about the energy and the dissociation channel of the first peak in the DEA cross section for NO_2.

Despite several experimental studies of the DEA to NO_2, theoretical interpretation of the experimental data is very limited. In their *R*-matrix calculation Munjal *et al* [16] reported that NO_2^- has two shape resonances of $^3B_1$ and of $^1B_1$ symmetry at 1.18 eV and 2.3 eV, respectively, which are responsible for the O^- channel of DEA at low scattering energies. To the best of our knowledge, a theoretical cross section for DEA to NO_2 has not yet been reported. Recently, Yuen *et al* [17] developed a simplified model, inspired by the theoretical approach of O'Malley and Bardsley [18–20], to estimate DEA cross sections for polyatomic molecules. In the present work we adapt that model to investigate the electron attachment to NO_2.

In the following section our theoretical approach is presented. The cross section for electron capture by the NO_2 molecule is presented in section 3. In section 4 we consider autodetachment that reduces the attachment cross section. The concluding remarks are given in section 5.

2. Theoretical approach

The process of DEA in NO_2 mediated by electronic resonant states of the negative molecular ion can be described as following:

$$NO_2(X^2A_1) + e^- \rightarrow NO_2^{-*}(^{1,3}B_1) \rightarrow O^-(^2P) + NO(X^2\Pi). \quad (1)$$

A schematic view of the process is shown in figure 1. The black and green solid curves are the potential energy surfaces (PESs) of NO_2 and NO_2^{-*} as functions of the symmetric stretching coordinate. The NO_2 molecule captures the incident electron forming a temporary anion NO_2^{-*}. When the vibrating molecule stretches beyond the crossing point q_s between

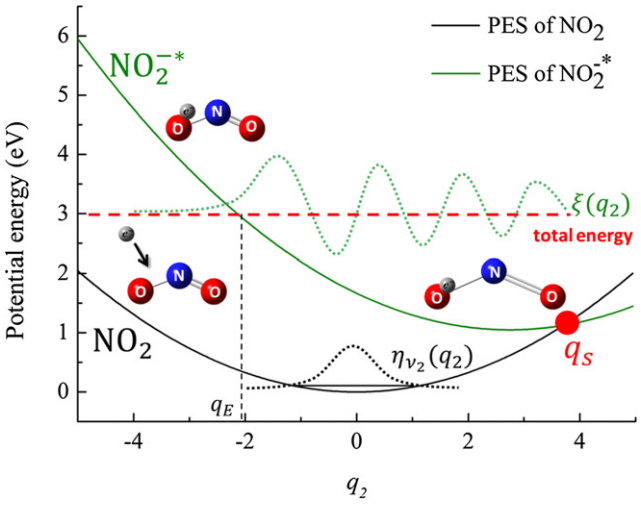

Figure 1. Schematic view of electron attachment to NO_2. The PES of NO_2 (black solid line) is plotted as $\hbar\omega_2 q_2^2/2$, where q_2 is the coordinate for symmetric stretching and ω_2 is the harmonic vibrational frequency. The PES of NO_2^{-*} (green solid line) is obtained by adding the resonance energy to the NO_2 PES. The black and green dotted curves are the nuclear wave functions ξ and η_{ν_2} of NO_2 and NO_2^{-*}, respectively. The black horizontal line represents the zero-point energy of NO_2. The red dashed line represents the total energy (E) of the system, which is the energy of the target molecule plus the electron scattering energy ε.

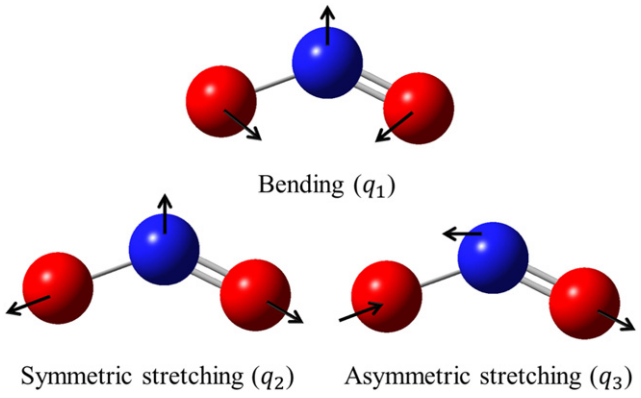

Figure 2. Three different normal modes of NO_2. The arrows indicate the force vectors.

the PESs of NO_2 and NO_2^{-*}: the anion becomes stable. Then, the system could dissociate into the fragments $O^- + NO$ or, as a second possibility, the vibrating anion can return back to geometries, where detachment of the electron is again possible so that there is a possibility for autodetachment.

In order to determine the capture coordinate of the system as in reference [17], we first determined normal modes and corresponding harmonic frequencies of NO_2 using MOLPRO [21]. NO_2 has three normal modes: bending, symmetric stretching, and asymmetric stretching as shown in figure 2. Corresponding dimensionless normal coordinates are denoted by q_1, q_2, and q_3 respectively. Then, the resonance energy of the $e^- + NO_2$ system as a function of displacements along normal modes is calculated by the UK *R*-matrix program [22] with the Quantemol-N interface [23]. The scattering calculations employed the correlation consistent polarized valence triple zeta (`cc-pVTZ`) basis set to

Table 1. Parameters of the lowest two resonances obtained at the equilibrium geometry. Comparison with that of Munjal *et al* [16] is also shown in the table. Positions and widths of the resonances are denoted by Δ and Γ, respectively.

	Present work		Munjal *et al* [16]	
Symmetry	Position Δ (eV)	Width Γ (eV)	Position Δ (eV)	Width Γ (eV)
$^3B_1$	1.65	0.11	1.178	0.083
$^1B_1$	2.93	0.25	2.33	0.15

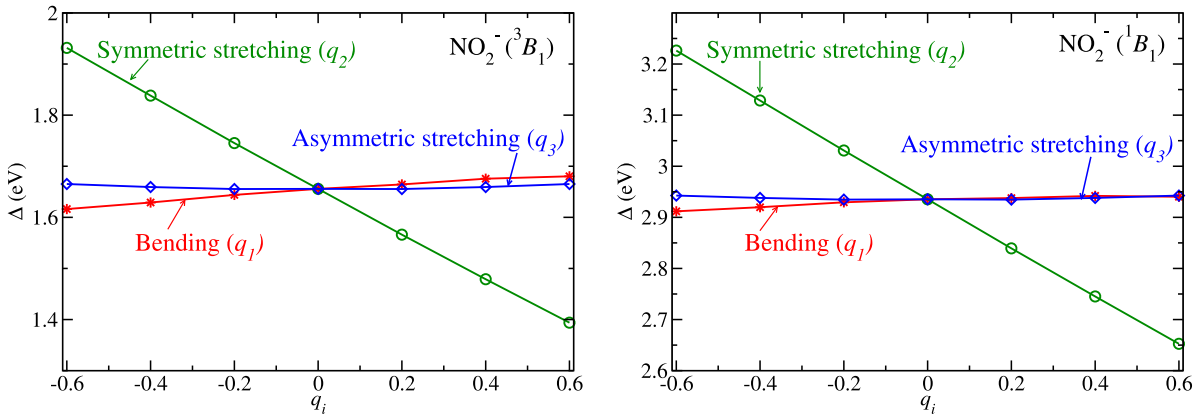

Figure 3. Resonance energies Δ as functions of q_1 (red asterisks), q_2 (green circles) and q_3 (blue diamonds) of the $^3B_1$ and $^1B_1$ states of NO_2^-.

describe the target. A complete active space configuration interaction representation was used, where 10 electrons are frozen in the core orbitals $1a_1, 2a_1, 3a_1, 1b_2, 2b_2$ and remaining 13 electrons are distributed freely in an active space of $4a_1, 5a_1, 3b_2, 1b_1, 4b_2, 1a_2, 6a_1, 7a_1, 2b_1$, and $5b_2$. The radius of the R-matrix sphere is 14 bohrs and all the target states below the cut-off energy of 10 eV are retained in the close-coupling expansion. The resonance position Δ and the width Γ are determined by fitting the computed eigenphase sums with the Breit–Wigner formula [24]. More computational details could be found in reference [25].

Table 1 shows parameters of resonances found below 4 eV at the equilibrium geometry. Energies of the first and second resonances are 1.65 and 2.93 eV, which agree with the location of the first two peaks of the experimental DEA cross section. Comparing with the theoretical study by Munjal *et al* [16], the present resonance energies are larger by about 30% and 20% for the $^3B_1$ and the $^1B_1$ resonances.

Figure 3 shows the resonance energy Δ of the $^{1,3}B_1$ state as a function of different normal-mode coordinates. We found that for the bending mode (q_1) and the asymmetric stretching mode (q_3), the resonance energy Δ is nearly constant near the equilibrium geometry. In contrast, there is a significant variation along the symmetric stretching mode (q_2). It means that if the NO_2^- anion dissociates after the attachment step, the dissociation starts with sliding down the PES of the $^1B_1$ or $^3B_1$ states along the q_2 coordinate.

The PESs of NO_2 and $^3B_1$ state of NO_2^- as functions of the normal coordinates are also shown in figure 4. The PES of the resonant state is obtained by adding the resonance energies to the neutral state PES (see equation (5)). Because the resonance energies are nearly constant along q_1 and q_3, the PES of the $^3B_1$ state of NO_2^- in the space of the q_1 and q_3 coordinates is almost parallel to the NO_2 PES, (see the left panel of figure 4). In contrast, the PES of NO_2 crosses the $^3B_1$ PES of NO_2^- as q_2 increases (see the right panel of figure 4). Therefore, one can reduce the multidimensional nuclear dynamics of NO_2^- to the dynamics along the q_2 coordinate only, similarly to the scheme of figure 1.

Since only one normal mode coordinate q_2 is responsible for the nuclear motion away from the NO_2 equilibrium once the electron is attached to the target, no transformation is needed for the coordinates as it was done in reference [17]. The attachment cross section is given by the O'Malley formula [17, 18] for one-dimensional motion

$$\sigma_{\rm cap}(\varepsilon) = \sum_d g_d \frac{2\pi^2}{k^2} \frac{\Gamma_d(q_\varepsilon)}{|U_d'(q_E)|} |\eta_{\nu_2}(q_E)|^2, \qquad (2)$$

where the sum is taken over the two resonances $d = ^3B_1$ and $^1B_1$, $k = \sqrt{2m_e\varepsilon}/\hbar$ is the wave number of the incident electron and g_d is the spin statistical ratio with $g = \frac{3}{4}$ for $^3B_1$ and $g = \frac{1}{4}$ for $^1B_1$, q_ε and q_E are the Frank–Condon point and the classical turning point, which are obtained by solving $\Delta_d(q_\varepsilon) = \varepsilon$ and $U_d(q_E) = E$ (see figure 1), respectively [17].

3. Cross section for electron capture

To evaluate the attachment cross section, one needs the resonance energies Δ_d and widths Γ_d, the PESs U_d of the resonant anion, and the initial nuclear wave function η_{ν_2} of the target. The resonance energies and PESs for the $^3B_1$ and $^1B_1$ states

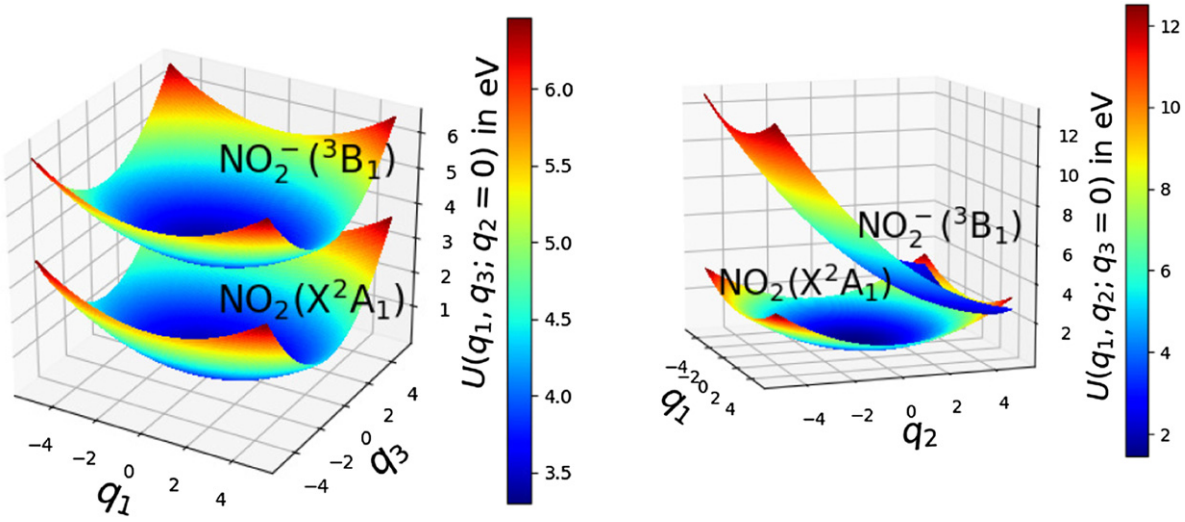

Figure 4. PESs of NO_2 and NO_2^- over the three normal coordinates. The left panel shows the PES of the ground electronic state X^2A_1 of NO_2 and the PES of the $^3B_1$ state of the anion in the q_1 and q_3 coordinates. The right panel shows the same PESs in the space of q_1 and q_2. On the right of the two panels, the color scales refer to the $^3B_1$ resonant state.

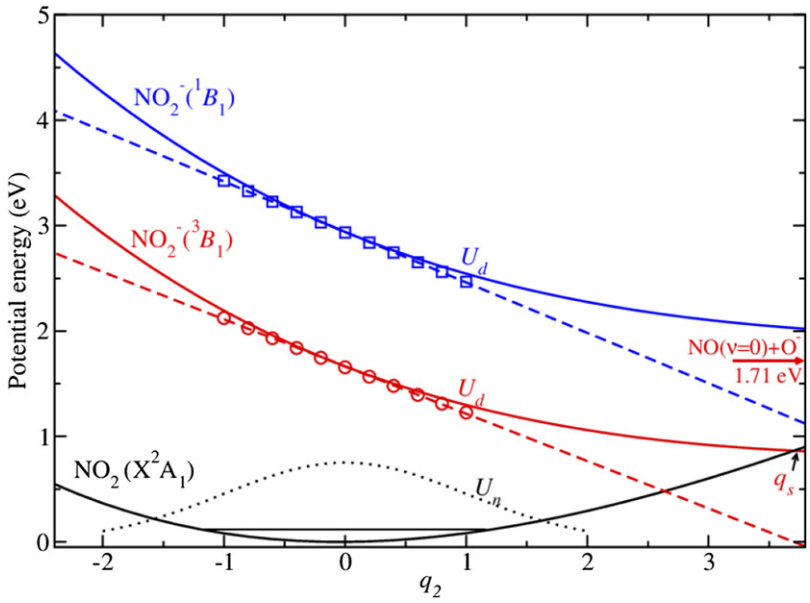

Figure 5. PESs of NO_2 and NO_2^- as functions of the q_2 normal mode. The black curve is the PES U_n of the NO_2 ground state. The red and blue curves are the potential energies U_d for $^3B_1$ and $^1B_1$ resonance states, respectively. The $^3B_1$ and $^1B_1$ resonance energies Δ, obtained in the R-matrix calculation, are shown by red circles and blue squares and linear fits are shown with dashed lines of the same colors. The arrow indicates the theoretical dissociation limit correlated to $NO(v = 0) + O^-$ of NO_2^- ($^3B_1$).

along q_2 are displayed in figure 5. The dashed lines show the linear approximation of $\Delta_d(q_2)$,

$$\Delta_d(q_2) \approx \Delta_d(0) + \frac{d\Delta_d}{dq_2} q_2, \tag{3}$$

where $d\Delta_d/dq_2$ is the slope of the resonance energy over q_2. The widths of the $^3B_1$ and the $^1B_1$ resonances at different q_2 are shown in figure 6 and are fitted as

$$\Gamma_d = \alpha_d \left(\Delta_d(0) + \frac{d\Delta_d}{dq_2} q_2 \right)^{\beta_d}. \tag{4}$$

The values of the fitting parameters are given in table 2. One can see that the widths go to zero at around $q_2 = 3.7$ and 6.1 for the $^3B_1$ and the $^1B_1$ resonances, respectively, such that stabilization occurs far from the Franck–Condon region. The PESs of NO_2^- are obtained by

$$U_d(q_2) = U_n(q_2) + \Delta_d(q_2) = \frac{\hbar\omega_2 q_2^2}{2} + \Delta_d(q_2). \tag{5}$$

Finally, the nuclear wave function η_{ν_2} of the NO_2 molecule in the ground vibrational state is approximated with a Gaussian function normalized in q_2.

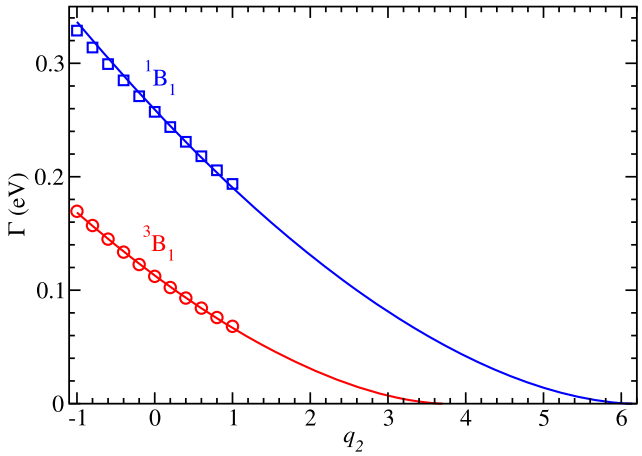

Figure 6. Widths of the $^3B_1$ (red circles) and the $^1B_1$ (blue squares) resonances as functions of the normal coordinate q_2. The solid curves are analytical fits of equation (4).

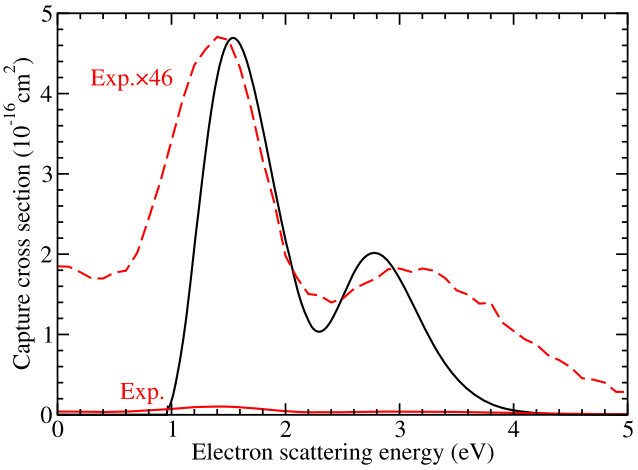

Figure 7. The cross section for the electron attachment to NO_2 calculated by equation (2) (black curve). The red solid curve is the NO_2 DEA cross section measured by Rangwala *et al* [13] and the red dashed curve is the same cross section multiplied by a factor of 46.

Table 2. Parameters of the fitted widths.

Γ	α	β	$d\Delta/dq_2$
$^3B_1$	0.048 2288	1.672 69	−0.448 79
$^1B_1$	0.040 0452	1.731 67	−0.478 67

The computed attachment cross section is given in figure 7. The threshold in the cross section around 1 eV is related to the energy-dependent Franck–Condon factor in equation (2), rather than to the NO($v = 0$) + O^- threshold energy 1.71 eV, computed in this study. This is because we did not consider the nuclear dynamics of the NO_2^- system beyond the Franck–Condon region in equation (2). The overall shape of the attachment cross section is in good agreement with the experiment [13], which suggests that the present theory describes well the electron-attachment process. However, the peak value of the cross section is about 46 times larger than the experimental DEA cross section measured by Rangwala *et al* [13]. This could mean that the largest part of the outgoing flux in the dissociating NO_2^- anion returns back and the anion is destroyed by autodetachment. In other words, it could mean that the probability of survival of the anion with respect to autodetachment is small.

4. Accounting for autodetachment

Because the widths of the resonances Γ_d are of the order of 0.1 eV (see table 1), autodetachment is not negligible and should be accounted for when the DEA cross section is calculated. The DEA cross section can be written as a product of the attachment cross section $\sigma_{\rm cap}$ and a survival probability $P_{\rm s}$. As a result, the DEA cross section is estimated as $\sigma_{\rm DEA} \approx \sigma_{\rm cap} P_{\rm s}$.

Using the WKB approximation, the survival probabilities $P_{\rm s}$ are approximated as [18, 26, 27]

$$P_{\rm s} = \exp\left(-\frac{1}{\hbar}\int_{t_E}^{t_{\rm s}} \Gamma(q_2)dt\right) = \exp\left(-\int_{q_E}^{q_{\rm s}} \frac{\tilde{\Gamma}(q_2)}{\tilde{v}(q_2)}dq_2\right), \tag{6}$$

where $\tilde{\Gamma} = \Gamma/(\hbar\omega_2)$ is the dimensionless resonance width and $\tilde{v}(q_2) = \sqrt{2\left[(E - U_d(q_2))/(\hbar\omega_2)\right]}$ is the dimensionless velocity. The integration is performed in the region between the classical turning point q_E and the stabilization point $q_{\rm s}$.

The calculated survival probabilities $P_{\rm s}$ are plotted in figure 8. The two curves have different thresholds with energies $E = U_d(q_{\rm s})$: if the total energy, E, is smaller than the energy $U_d(q_{\rm s})$, where the resonant curve crosses the ionic curve, the survival probability is set to zero. The overall survival probability for the $^1B_1$ state is smaller than that for the $^3B_1$ state, because the width of the $^1B_1$ state is larger than that of the $^3B_1$ state and the stabilization point $q_{\rm s} = 6.1$ of the $^1B_1$ state is further away than for the $^3B_1$ state, $q_{\rm s} = 3.7$ (see figure 5).

To account for the energy threshold for the DEA to NO_2, we further multiplied a Heaviside function $\theta(E - E_{\rm th})$ to the DEA cross section, such that

$$\sigma_{\rm DEA}(\varepsilon) \approx \sigma_{\rm cap}(\varepsilon)\, P_{\rm s}(\varepsilon)\, \theta(E - E_{\rm th}), \tag{7}$$

where $E_{\rm th} = 1.71$ eV is the NO($v = 0$) + O^- threshold energy mentioned above.

The resulting computed DEA cross section is shown with the solid line in figure 9. The dot-dashed (blue) line shows the theoretical cross section convoluted with the experimental uncertainty of 0.5 eV in the electron energy [13]. The first peak of the cross section in the present study is 2×10^{-16} cm^2 at 1.71 eV. The position of the low-energy resonance is shifted to

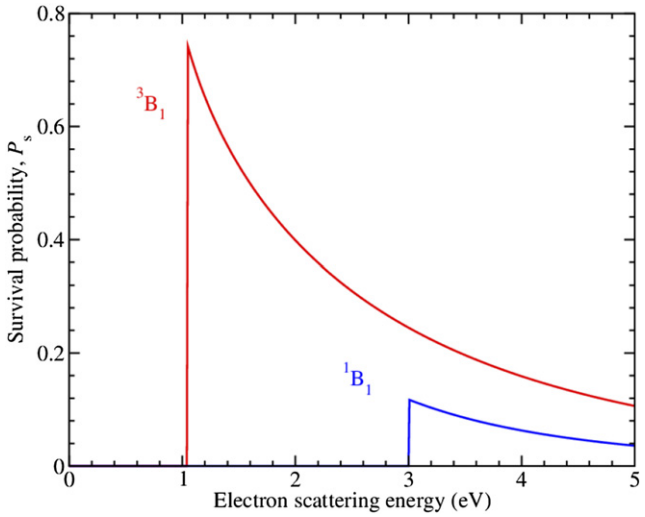

Figure 8. Survival probability of the $^3B_1$ (red curve) and the $^1B_1$ (blue curve) resonances as functions of the electron scattering energy.

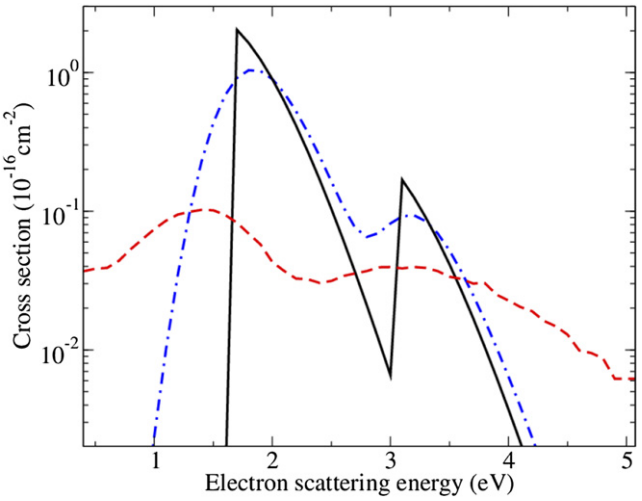

Figure 9. Comparison of the raw, convoluted, and experimental DEA cross sections. The solid line (black) is the raw theoretical cross section. The dot-dashed (blue) line is the cross section convoluted with $\Delta E = 0.5$ eV. The experimental results obtained by Rangwala *et al* [13] are shown by the dashed (red) line.

the right by about 0.3 eV with respect to the experimental value by Rangwala *et al* [13] and the magnitude is about ten times larger. The position of the second peak at 3.0 eV, observed by Rangwala *et al* [13], is well reproduced in the present study, but the magnitude of the theoretical cross section is about two times larger than in the experiment. The uncertainty in position and width of the calculated resonances due to the theoretical model are about 20%. The uncertainty was estimated by changing the basis set and the CAS used in the calculations. Therefore, the difference in the magnitude of the theoretical and experimental cross sections cannot be explained by the uncertainty of the theoretical model.

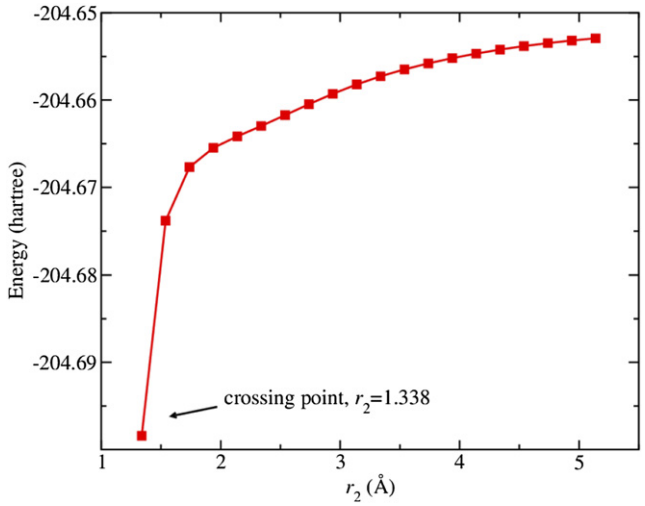

Figure 10. MEP of the $^3B_1$ state ($^3A''$ for the C_s geometries) of NO_2^- from the crossing point towards the dissociation limit NO + O^-.

The disagreement with the experimental cross section could possibly be explained by a potential barrier, if it exists, in the dissociation pathway NO + O^-. To verify the existence of the barrier, we computed the minimum energy pathway (MEP) of the $^3B_1$ state of NO_2^- from the crossing point q_s in figure 5 towards the dissociation limit NO + O^- using the multi-reference configuration interaction (MRCI) method from MOLPRO. As a first step, we used the spin-restricted Hartree–Fock (HF) method to determine the electronic structure of NO_2^- in the ground state with the `aug-cc-pVTZ` basis set. The electronic configuration of NO_2^- ($^1A'$) represented in the C_s symmetry is found to be $(1-8a')^2(1a'')^2(9a')^2(2a'')^2(10a')^2$. With the HF orbitals, we constructed the $^3A''$ state of NO_2^- (corresponding to the $^3B_1$ state in the C_{2v} symmetry) using the CASSCF method, where four electrons in the $2a''$ and $10a'$ orbitals are freely distributed among the $10–11a'$ and $2–3a''$ orbitals. Finally, the MRCI calculation for $NO_2^-(^3A'')$ was performed using the orbitals from the CASSCF calculation. Figure 10 shows the MEP for the lowest ($^3A''$) state of NO_2^-. Each energy point is obtained by optimizing the MRCI energy with respect to one of the NO bond lengths and the ONO angle, while the other NO bond length is fixed at a given value of r_2. One can see that the MEP energy approaches the dissociation limit at $r_2 > 5$ Å from below without a potential barrier. Therefore, the lowest $^3A''$ state, which is the same as the $^3B_1$ state discussed above, has a threshold energy, but no potential barrier.

5. Summary

To summarize, we modeled the process of attachment of a low-energy electron to the NO_2 molecule in the ground

vibrational level. The symmetric stretching mode of NO_2 was found to contribute the most to the process. The attachment cross section was computed using an approach based on the O'Malley theory, developed in 1960s for diatomic molecules, and generalized to polyatomic molecules by Yuen *et al* [17]. After taking into account the autodetachment and dissociation thresholds, DEA cross section of NO_2 was evaluated. Positions of the two resonances, obtained in the study, agree well with the experiment. Peak values of the convoluted cross section at energies of the two resonances are larger by factors of 10 and 2 compared to the experiment by Rangwala *et al* [13]. The shape of the convoluted cross section agrees quite well with the experiment. To understand the discrepancy between the theory and the experiment, the MEP of the $^3B_1$ state of NO_2^- towards the dissociation limit NO + O^- was determined. No potential barrier was found.

We concluded that our model probably overestimates the DEA cross section for NO_2. Experiments with a better energy resolution as well as a more accurate theoretical approach are therefore needed to further access the applicability and accuracy of the present DEA theory for NO_2. A multidimensional wave-packet propagation method is an example of more accurate theoretical approach. This method can account for the effect of multidimensional nuclear dynamics. The method required global PESs of the resonant states. Computing the resonant anion PES is a laborious task. The approach presented here provides a simpler way to estimate the DEA cross section. For systems with the dissociation pathway on a single PES or even multiple coupled PES, having no barrier to dissociation, the current approach can be applied in a straightforward manner. Therefore, it is highly desirable to continue to benchmark the current theoretical approach on other polyatomic molecules.

Acknowledgments

Hainan Liu and Xianwu Jiang contributed equally to this work. This work was supported by the China Scholarship Council, the Thomas Jefferson Fund of the Office for Science and Technology of the Embassy of France in the United States and the National Science Foundation, Grant Nos. PHY-1806915 and PHY-2102188. It also received funding from the program 'Accueil des chercheurs étrangers' of CentraleSupélec and 'Séjour à l'étranger 2019' of école doctorale INTERFACES of Université Paris-Saclay. The authors are grateful for the helpful discussion with Profs. Pietro Cortona from CentraleSupélec and Samantha Douguet from Rollins College.

Data availability statement

No new data were created or analysed in this study.

ORCID iDs

Chi-Hong Yuen https://orcid.org/0000-0002-0544-4976
Viatcheslav Kokoouline https://orcid.org/0000-0002-9945-0858
Mehdi Ayouz https://orcid.org/0000-0002-0447-5551

References

[1] Chmielewski A G 2007 *Radiat. Phys. Chem.* **76** 1480–4
[2] Chang J S 2008 *Plasma Sources Sci. Technol.* **17** 045004
[3] Chmielewski A G and Han B 2017 (Berlin: Springer)
[4] Srivastava R K, Hall R E, Khan S, Culligan K and Lani B W 2005 *J. Air Waste Manage. Assoc.* **55** 1367–88
[5] Wolford M F, Myers M C, Hegeler F and Sethian J D 2013 *Phys. Chem. Chem. Phys.* **15** 4422–7
[6] Petrova T B, Petrov G M, Wolford M F, Giuliani J L, Ladouceur H D, Hegeler F, Myers M C and Sethian J D 2017 *Phys. Plasmas* **24** 023501
[7] Misra N, Schlüter O and Cullen P J 2016 *Cold Plasma in Food and Agriculture: Fundamentals and Applications* (New York: Academic)
[8] Shimizu T *et al* 2008 *Plasma Process. Polym.* **5** 577–82
[9] Fox R E 1960 *J. Chem. Phys.* **32** 285–7
[10] Rallis D A and Goodings J M 1971 *Can. J. Chem.* **49** 1571–4
[11] Stockdale J A D, Compton R N, Hurst G S and Reinhardt P W 1969 *J. Chem. Phys.* **50** 2176–80
[12] Abouaf R, Paineau R and Fiquet-Fayard F 1976 *J. Phys. B: At. Mol. Phys.* **9** 303
[13] Rangwala S A, Krishnakumar E and Kumar S 2003 *Phys. Rev.* A **68** 052710
[14] Nandi D and Krishnakumar E 2010 *Int. J. Mass Spectrom.* **289** 39–46
[15] Gope K, Tadsare V, Prabhudesai V S and Krishnakumar E 2017 *Eur. Phys. J.* D **71** 1–6
[16] Munjal H, Baluja K and Tennyson J 2009 *Phys. Rev.* A **79** 032712
[17] Yuen C, Douguet N, Dos Santos S F, Orel A and Kokoouline V 2019 *Phys. Rev.* A **99** 032701
[18] O'Malley T F 1966 *Phys. Rev.* **150** 14
[19] Bardsley J N 1968 *J. Phys. B: At. Mol. Phys.* **1** 365
[20] Bardsley J N 1968 *J. Phys. B: At. Mol. Phys.* **1** 349
[21] Werner H-J, Knowles P J, Knizia G, Manby F R and Schütz M 2012 *Wiley Interdiscip. Rev.-Comput. Mol. Sci.* **2** 242–53
[22] Tennyson J 2010 *Phys. Rep.* **491** 29–76
[23] Tennyson J, Brown D B, Munro J J, Rozum I, Varambhia H N and Vinci N 2007 *J. Phys.: Conf. Ser.* **86** 012001
[24] Tennyson J and Noble C J 1984 *Comput. Phys. Commun.* **33** 421–4
[25] Liu H, Dos Santos S F, Yuen C H, Cortona P, Kokoouline V and Ayouz M 2019 *Plasma Sources Sci. Technol.* **28** 105017
[26] Bardsley J N, Herzenberg A and Mandl F 1966 *Proc. Phys. Soc.* **89** 321
[27] Chen J C Y 1966 *Phys. Rev.* **148** 66